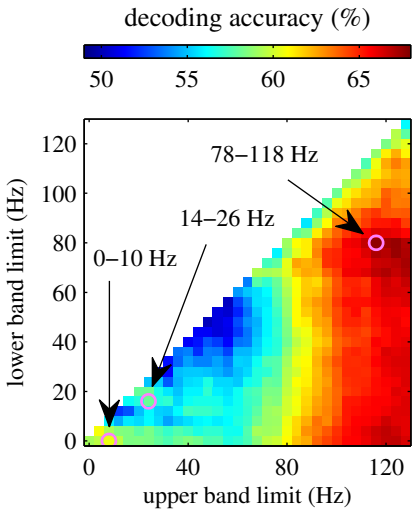

Fig. SUP1. Decoding of object weight from frequency band modulations. Average over all subjects. An analysis for all possible average frequency bands between 0 and 128 Hz, corresponding to Fig. 3c for grasp type, was done using amplitude samples from all hand-arm channels at seven time points, from 0.5 s before until 1 s after grasp onset. Three separate frequency bands exhibiting local maxima, indicted by pink circles, have been selected based on this analysis for weight decoding. Comparing these results to those for grasp type decoding as shown in Fig. 3c, some common features can be observed. In both cases, a low frequency band and a broad high frequency band were found to perform relatively well, while intermediate frequencies had very little predictive power. Those bands found to be best suited for weight decoding were slightly shifted as compared to those in grasp type decoding. Most notably, an intermediate frequency band in the low beta-range (14-26 Hz) was found to perform better than the high beta range (cf. Fig. 3). However the variability across subjects was rather high in these intermediate frequencies (not shown). Please note that the colour scale is different from Fig. 3c, since decoding accuracy for weight was generally lower than for grasp type.

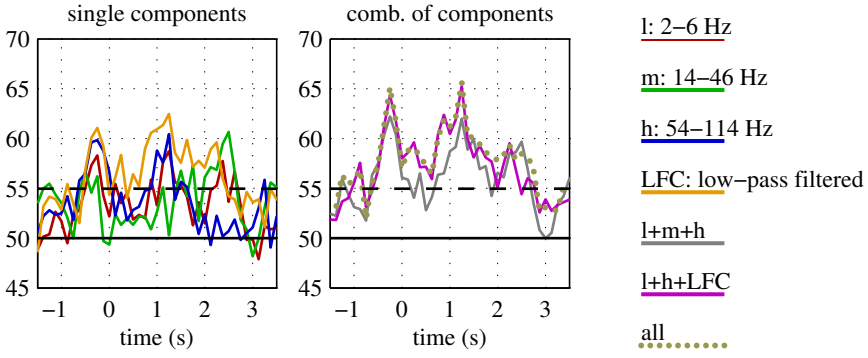

Fig. SUP2. Temporal development of decoding accuracy of object weight.

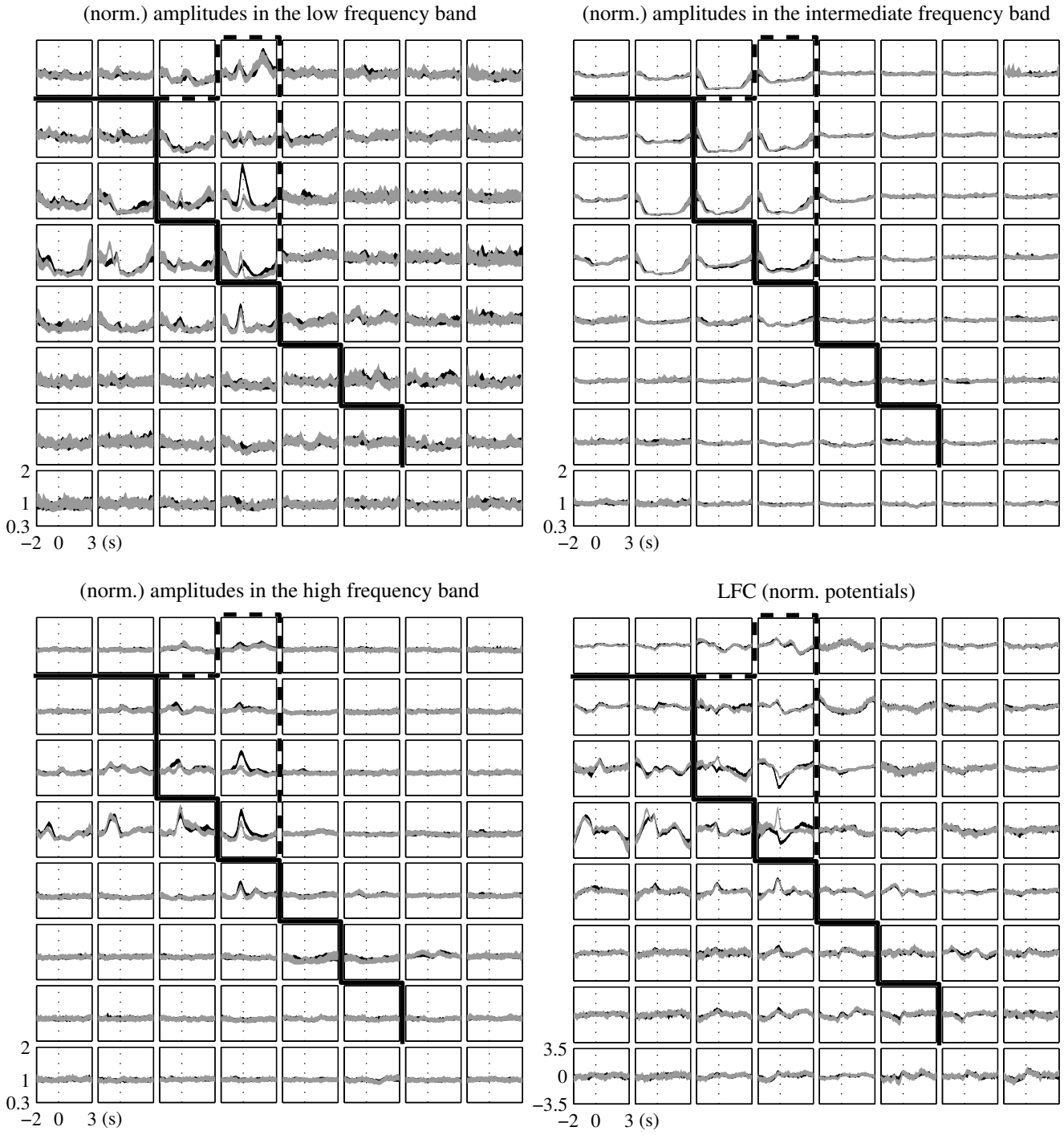

Fig. SUP3. Average feature modulations (±3×SEM, cf. Fig. 4) of S1, all channels from the implanted 8×8 electrode grid are shown. Normalized amplitude modulations in a low (2-6 Hz), an intermediate (14-46 Hz) and a high (54-114 Hz) frequency band, as well as normalized potentials of the low-pass filtered component (LFC) are depicted. Solid lines separate electrode positions posterior and anterior to the central sulcus (anterior to the upper right, posterior to the lower left), electrodes on the hand-arm motor area are marked by a dashed outline.

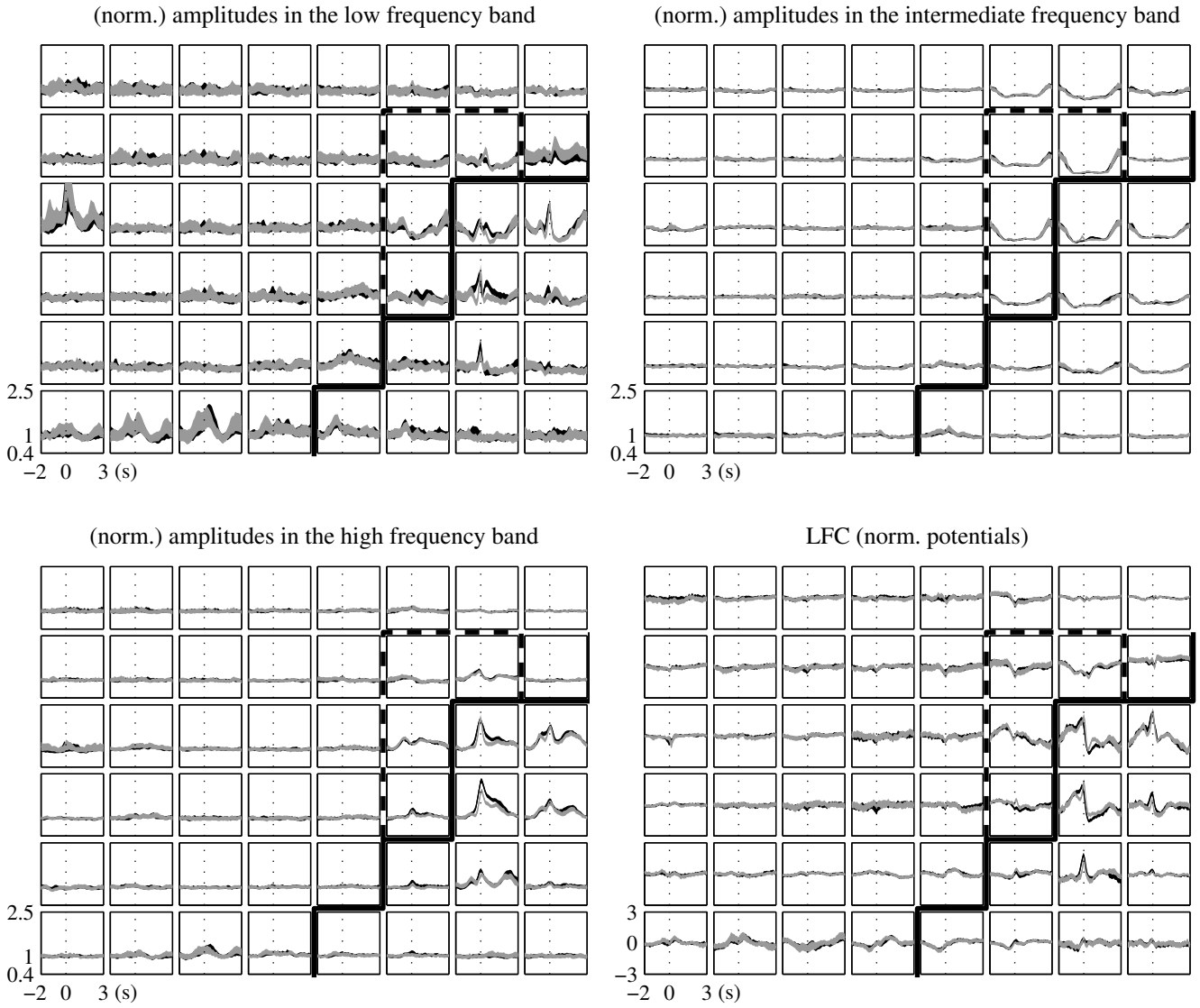

Fig. SUP4. Average feature modulations (±3×SEM) of S2, all channels from the implanted 8×6 grid of electrodes are shown. All conventions as in Fig. SUP2, except for anterior corresponding to the upper left and posterior to the lower right.

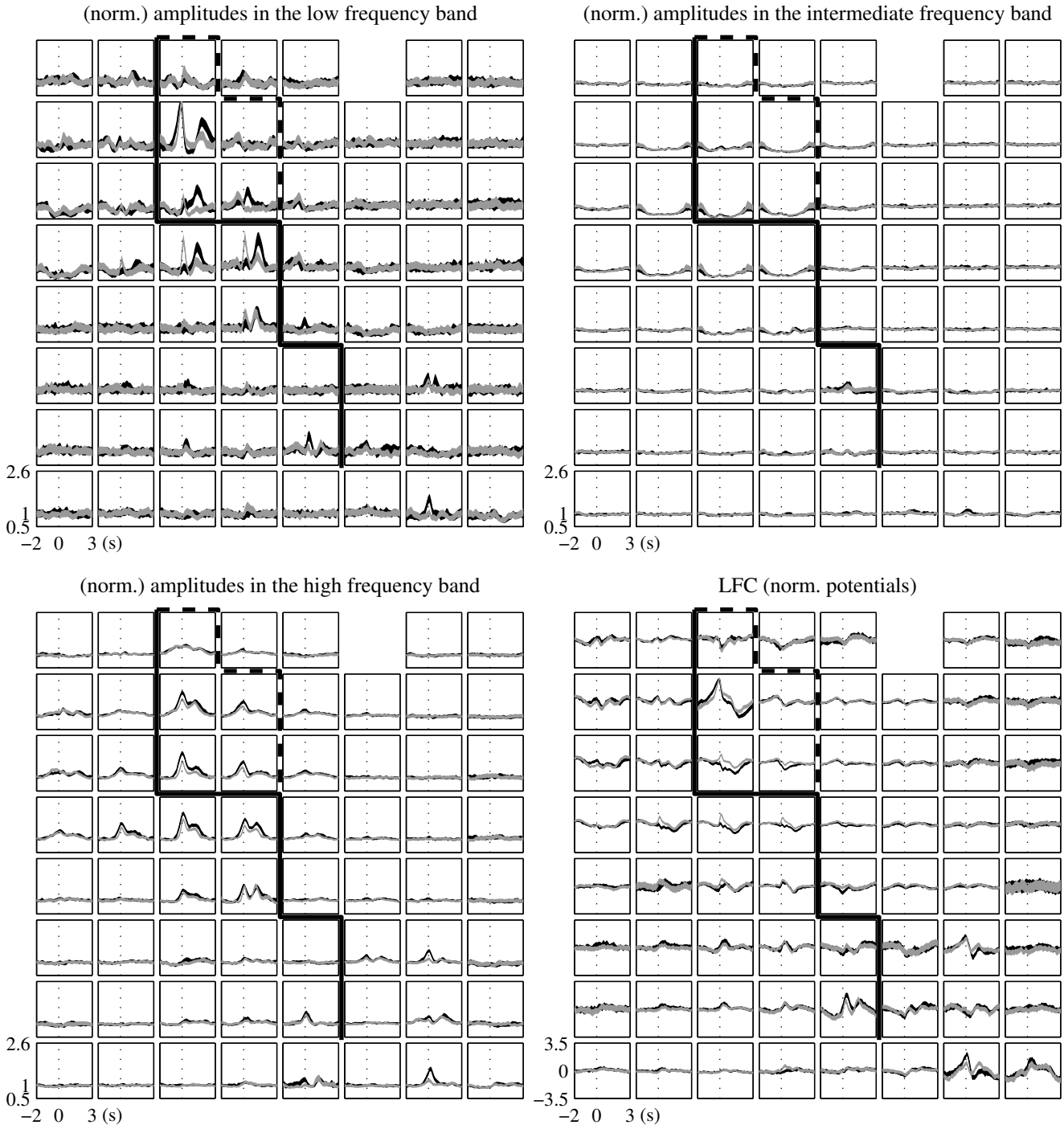

Fig. SUP5. Average feature modulations (±3×SEM) of S3. All conventions as in Fig. SUP2.

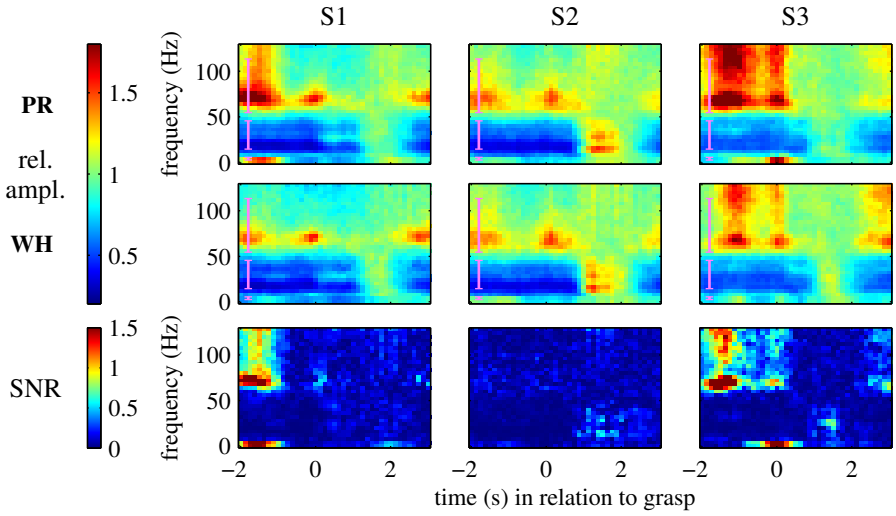

Fig. SUP6. Average spectrograms and signal-to-noise ratio (SNR), aligned on the time point of cup release (t = 0) shown for one representative channel from hand-arm motor cortex of each subject (from left to right: S1-S3). Top row: average over all trials using precision grip (PR). Second row: whole-hand grip (WH). Bottom row: SNR over both conditions (cf. Fig. 3). Note that the second time period of high frequency responses, which is also visible in Fig. 3, is related to cup release, hence becoming sharper and more pronounced when aligned to this event. Except for the alignment to cup release rather than grasp onset, analysis was identical to that for Fig. 3a-b.

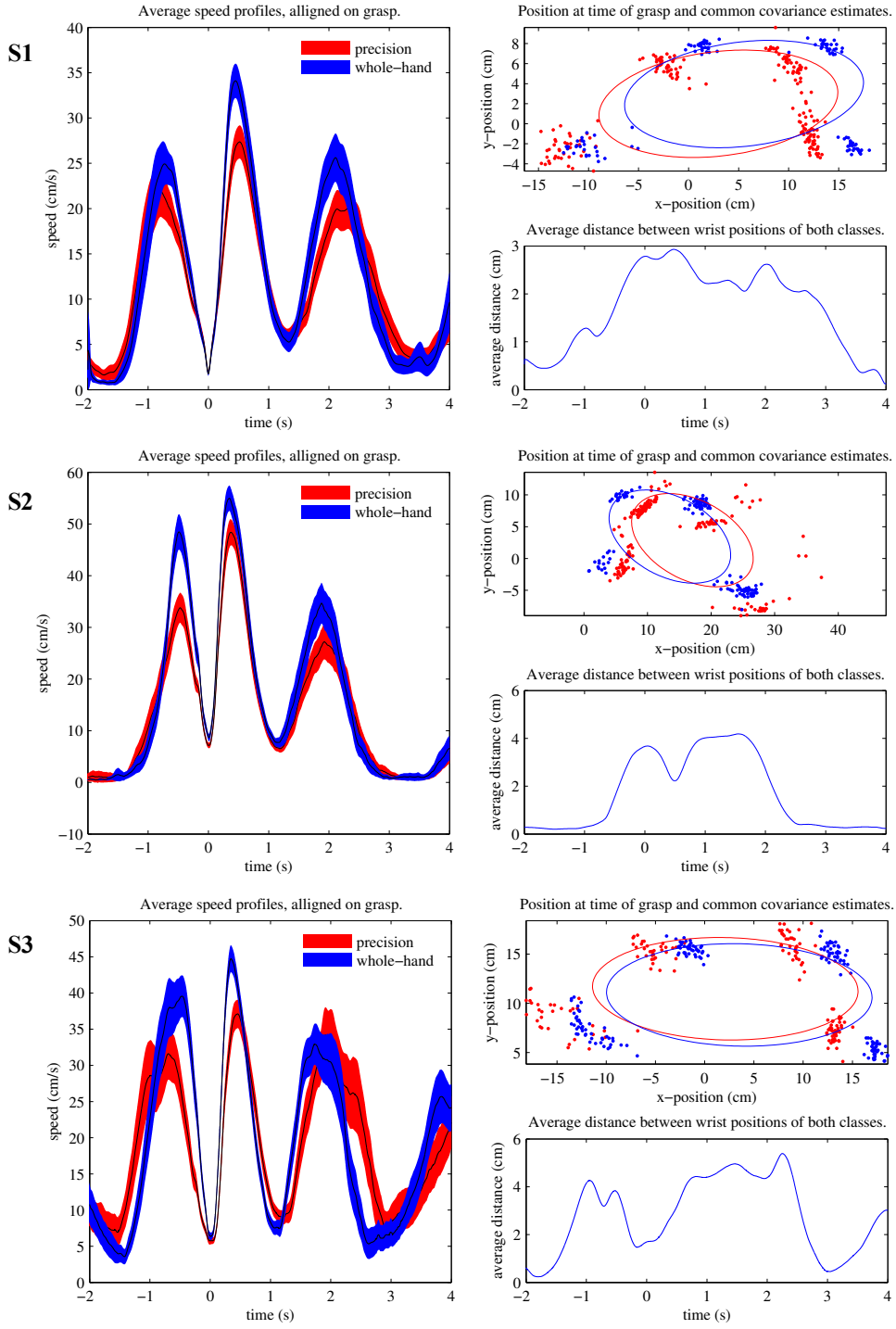

Fig. SUP7. Grasp-specific differences in arm kinematics as recorded by the movement tracking device. Left panel of each subject: average speed profiles over the time course of a trial (aligned to grasp onset). Red (precision grip) and blue (whole-hand grip) bands denote average over trials ±1.96 × standard-error of the mean (to indicate significant differences). Top right panels: projection of wrist positions on the horizontal plane, at time of grasp, colour-coded for both grasp types. Ellipses indicate the 95% confidence regions of a Gaussian fit, with a common covariance matrix, as used in the RLDA (see Methods). Note that positions cluster around four locations, which are, however, unknown to the decoding process (which assumes Gaussian distribution). Lower right panels: average Euclidean distances between trials with precision and whole-hand grip over time. This demonstrates that grasp-specific differences are present also in the arm kinematics, which could potentially be exploited for indirect decoding of grasp types, if arm kinematics were well represented in the ECoG.

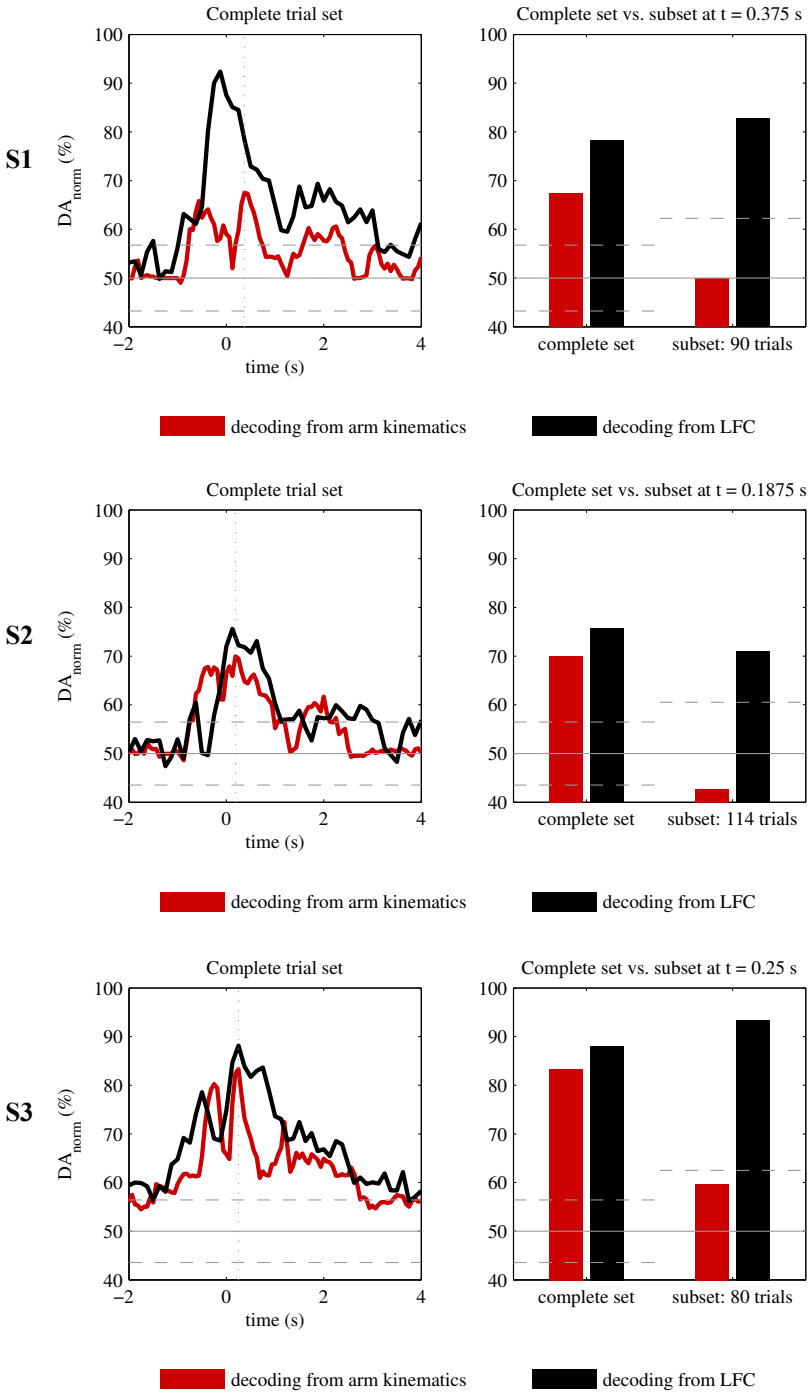

Fig. SUP8. Classification of grasp types from arm-kinematics. Left panels: Classification of grasp type at different time points (aligned on grasp onset). Red line: decoding accuracy (DA) using RLDA from the recorded arm kinematics, represented by a feature vector including x-, y-, and z-position, velocities in x-, y-, and z-directions, and total speed (= magnitude of the velocity vector). Speed provides additional information to the (linear) decoder since it cannot be inferred by a linear transformation. Black line: normalized DA using the same decoding scheme, but with a feature vector composed from LFC values of the ECoG from hand-arm motor channels. Horizontal solid and dashed lines indicate chance level, as well as upper and lower significance levels ($p < 0.01$). The dotted vertical line marks the time of peak DA for classification from arm kinematics. Right panels: Comparison of grasp type decoding at the time points indicated in the left panels, from arm kinematics (red) and LFC (black) over the complete set of trials vs. decoding from a subset of trials (right half). The trial subsets were chosen to minimize the distribution differences of arm kinematics between whole-hand grip and precision grip trials. This trial selection, exclusively optimized on arm kinematics, results in a DA below significance level for arm kinematics. DA for LFC from the same time point, however, based on this trial subset, stayed at a similar level. This strongly suggests that decoding from LFC primarily reflects differences in hand configuration and not (or only to a small amount) differences in arm kinematics. (Note that upper significance levels for decoding from the subsets are raised, due to a reduced number of trials.)

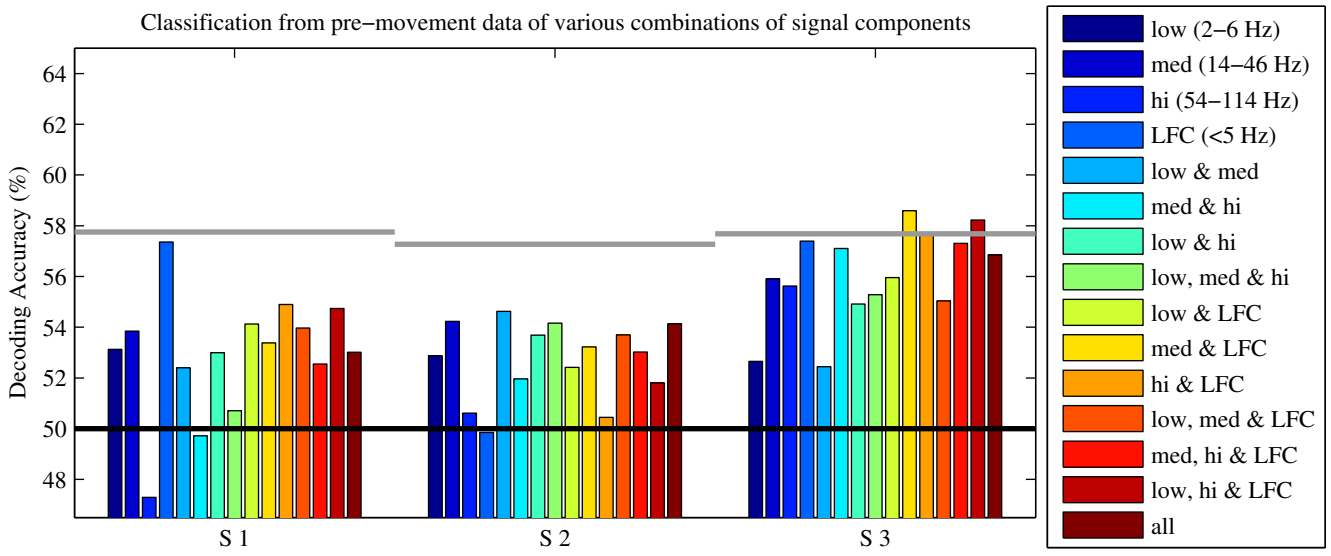

Fig. SUP9. Decoding from different signal components and from their combinations during a pre-movement period. Decoding of grasp types was based on ECoG signals from the resting period in between self-paced trials, composed of four values from time points from 500 to 125 ms before movement onset. For each subject (S1-S3), amplitudes in a low (2-6 Hz), intermediate (med, 14-46 Hz) and a high (hi, 54-114 Hz) frequency band, a low-pass filtered component (LFC) and all combinations of these four signal components were tested. The black line marks chance level, while grey lines show a significance level of $p < 0.003$ for each single test, which, according to Boole's inequality, for multiple testing with 15 different signal components and combinations yields an overall significance-level ≤ 0.05 (Bonferroni correction).

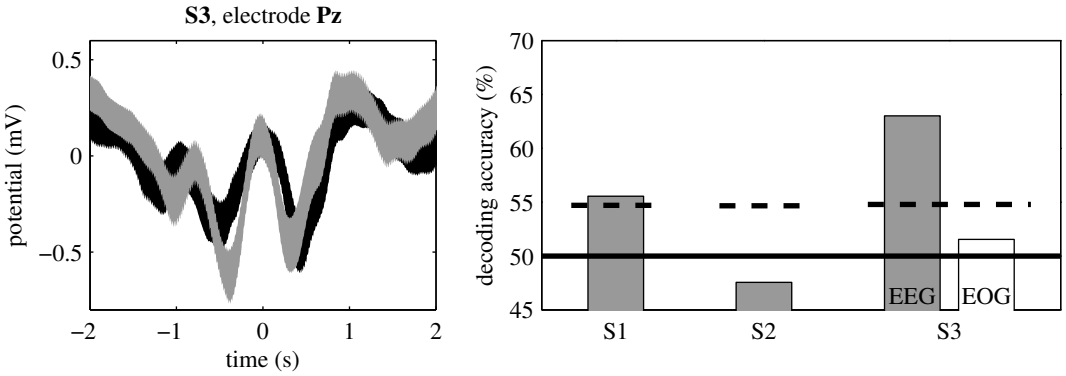

Fig. SUP10. Decoding of grasp modality from non-invasive EEG signals. (a) Average LFC potential of the EEG electrode with the highest grasp specific differences (Pz of S3): mean ± 1.96×standard error of the mean (95% confidence interval) for precision grip (black) and whole-hand grip (grey). (b) Decoding accuracy (DA) for classification from nine central EEG electrodes using the LFC from 1 second before to 0.5 seconds after time of grasp (sampled in 250 ms intervals). The solid black line marks chance level (50% DA), dashed lines show significance level ($p<0.05$). For S3: comparison with DA from EOG (white bar) as a control for possible influences of eye movements on decoding.

Classification of Grasp Type from Scalp EEG

For a comparison with non-invasive methods, we carried out the same approach of grasp type decoding as we used with the ECoG of hand-arm motor areas (section 3.2) with scalp-EEG recordings that were obtained synchronously with the ECoG. To minimize muscle and eye movement artefacts, while focusing on motor areas of the cortex, we restricted analysis to a selection of nine central electrodes at the following positions, according to the 10-20 system: F3, Fz, F4, C3, Cz, C4, P3, Pz and P4. Trials during which obvious artefacts were observed in EEG potentials were excluded from analysis. Fig. SUP11a shows the average LFC for both grasp types on the most discriminative channel found over all subjects, which was located at Pz in S3. Channels that were closer to those implanted ECoG contacts that were used for classification of grasp types, namely C3 (left hemisphere) or C4 (right hemisphere), however, did not show significant differences in the LFC between grasp types.

Single-trial decoding based on recordings from the nine central EEG electrodes , analogous to the decoding from the ECoG (cf. Fig. 5a), yielded DA significantly above chance level ($p<0.05$) for two subjects: S1, with 55.5 % and S3, with 63.0 % DA (Fig. SUP11b). The same procedure, but based on the EOG, resulted in a DA close to chance level, affirming that significant DA found for the EEG was unlikely to be caused by a contamination of eye movement artefacts.